The climate version of the Eta regional forecast model. 1. Evaluation of consistency between the Eta model and HadAM3P global model.

I. A. Pisnichenko* T.A. Tarasova*

25 November 2007

Abstract

The regional climate model prepared from Eta WS (workstation) forecast model has been integrated over South America with the horizontal resolution of 40 km for the period of 1960-1990. The model was forced at its lateral boundaries by the outputs of HadAM3P. The data of HadAM3P represent simulation of modern climate with the resolution about 150 km. In order to prepare climate regional model from the Eta forecast model multiple modifications and corrections were made in the original model as well as new program blocks were added. The run of climate Eta model was made on the supercomputer SX-6. The detailed analysis of the results of dynamical downscaling experiment includes an investigation of a consistency between the regional and AGCM models as well as of ability of the regional model to resolve important features of climate fields on the finer scale than that resolved by AGCM. In this work the results

*Centro de Previsão de Tempo e Estudos Climáticos/Instituto Nacional de Pesquisas Espaciais, Cachoeira Paulista, SP, Brazil, (pisnitch@cptec.inpe.br). Additional affiliation: A.M. Obukhov Institute of Atmospheric Physics, Russian Academy of Sciences, Moscow, Russia.

of the investigation of a consistency between the output fields of the Eta model and HadAM3P are presented. The geopotential, temperature and wind fields of both models were analysed. For the evaluation of the likeness of these two models outputs, there were used Fourier analysis of time series, consistency index, constituted from linear regression coefficients, time mean and space mean models' arithmetic difference and root mean square difference, dispersion analysis, and some others characteristics. This investigation demonstrates that there are not significant differences in behaviour and spatial arragement of large-scale structures of the two models. Also, the regional model characteristics do not have considerable positive or negative trend during integration time in relation to the global model characteristics. From the total analysis we can affirm that in the description of large-scale climate structures these two models are in consistency.

1. Introduction

The time averaged large-scale meteorological fields (>500 km) are actively studied in the works on climate theory and climate change analysis. Needs of agriculture, industrial and energy development planning require the knowledge of detailed, regional and local scale (100km - 10 km) climatic information. As the modern net of climate observation stations can supply data only suited for large-scale climate field investigations, the dynamical downscaling using high-resolution regional climate model (RCM) is the most powerful instrument for obtaining the smaller-scaled climate information. For the study of regional climate change in the future the dynamical downscaling is the only way to obtain necessary information. The dynamical downscaling approach involves RCM forced at the lateral and bottom boundaries by an atmospheric general circulation model (AGCM) or reanalysis data (e.g., Dickinson et al. 1989; Giorgi and Bates 1989). The finer regional-scale features of RCM can be attributed to detailed topography and land surface features, more comprehensive parameterization of unresolved physical

processes in the model equations, and explicit simulation of large mesoscale processes.

Atmosphere-ocean general circulation models (AOGCM) with the horizontal resolution of a few hundred kilometers are currently used for the simulation of large-scale response of the climate system to increasing of greenhouse gases and aerosol concentrations in the future. The running of RCM with the horizontal resolution of a few tens of kilometers over an area of interest with boundary conditions of AOGCM for the periods of 10-30 years in the present and in the future can give additional information about the regional-scale climate and climate-change effects in this area. Such downscaling studies related to climate change have been made already for various parts of Europe, North America, Australia, and Africa; see for example the references cited by Jones et al. (1997), Laprise et al. (2003), Giorgi et al. (2004), Duffy et al. (2006). Currently some large projects such as (PRUDENCE (Christensen et al. 2002) and NARCCAP (http://www.narccap.ucar.edu)), launched to investigate uncertainties in the RCM climate-change simulations over Europe and North America, are underway. Multiple regional climate model ensembles are used in these studies in order to minimize uncertainties obtained in simulations with each model.

The downscaling studies related to climate change over South America are just started. The project "Climate change scenarios using PRECIS" (Jones et al. 2004) was launched by Hadley Center for Climate Prediction and Research to develop user-friendly RCM which can be easily running on personal computer for any area of the globe. The South American countries including Brazil are participated in this project running PRECIS over various parts of South America. The data of the atmospheric global model HadAM3P were provided by Hadley Center for using them as boundary conditions in these simulations. The first regional climatology for South America is presented by Seth et al. (2007) for the period from 1982 to 2003. It was obtained by using the RegCM3 model (Pal et al. 2006) which was forced both by the reanalysis

data (Kanamitsu et al. 2002) and by the European-Hamburg (ECHAM) AGCM (Roeckner et al. 1996) global model.

The aim of this study is to propose one more regional climate model for use in the climate downscaling research over South America. For this aim we prepared the climate version from the NCEP Eta regional forecast model (Black 1994). The Eta Model was chosen because it was intensively used for weather forecast as well as for seasonal predictability and processes studies over South America during last decade (Figueroa et al. 1995; Tanajura 1996; Chou et al. 2000; Chou et al. 2002; Vernekar et al. 2003; Tarasova et al. 2006). Analysis of the integration results in most cases demonstrates better agreement with observations of meteorological fields simulated by the Eta model as compared with AGCM. Nevertheless, the longest integrations with the Eta model were limited to the continuous integrations for 3-5 months because of the limitations in the codes of the Eta model which was developed for the forecast studies. The climate versions of the Eta model which permit integrations for the period of any duration were developed at the Brazilian Instituto Nacional de Pesquisas Espaciais/ Centro de Previsao de Tempo e Estudos Cimaticos (INPE/CPTEC) during last years (Pisnichenko et al. 2006; Fernandez et al. 2006; Tarasova et al. 2006).

In order to be considered as a valid tool for dynamical downscaling of low-resolution GCM fields a regional climate model has to satisfy some requirements (e.g., Wang et al. 2004; Castro et al. 2005; Laprise, 2006). Firstly, it is needed to show that RCM is able to reproduce the principal features of the large-scale fields of GCM which data is used as driving boundary conditions and its main statistics. It is necessary condition indicating that nonlinear interactions of small-scale components do not strongly divert the system from the background state. This will also guarantee that boundary conditions do not transform into peculiarities. This is an issue of evaluation of consistency between RCM and GCM fields. Secondly, it is necessary to show

that RCM adds small-scale features absent in the GCM driving fields and that these features agree with observations and with high-resolution GCM fields. Laprise et al. (2007) provide a summary of studies related to this issue. On the opinion of Laprise et al. (2007) the consensus on the first point is not yet reached within the RCMs community. It is not clear if the large scales of GCM are unaffected, improved or degraded by RCMs. Note, that a comparison of large-scale fields of RCM and GCM is mainly performed for the surface temperature and precipitation (e.g., Hudson and Jones 2002; Seth et al. 2007). Another type of comparison is presented by Castro et al. (2005) for the one month simulation of Regional Atmospheric Modeling System RAMS (Pielke et al. 1992) with the boundary conditions of the reanalysis. They did the spectral analysis of the column average total kinetic energy and the column integrated moisture flux convergence and concluded from it that RAMS does not add increased skill to the large scale available in the reanalysis.

In this work we show the first results of our validation program related to the development of climate version of the Eta model. We investigated the consistency of the large-scale output fields of the Eta model and HadAM3P. For this, the geopotential, temperature and wind fields at various levels were analysed by using Fourier analysis of time series, consistency index, constituted from linear regression coefficients, time mean and space mean models' arithmetic difference (MAD), root mean square difference (RMSD), dispersion analysis and some others characteristics. The short description of the Eta model and the modifications, which we implemented in it, is given in Section 2. In this section the model integration procedure is also described. The newly developed version of the Eta model is hereafter termed as INPE Eta for Climate Change Simulations (INPE Eta CCS). Section 3 presents the results of the integrations with the INPE Eta CCS model over South America driven by boundary conditions from the HadAM3P for the period 1961-1991. The Eta model output fields are compared with those

from HadAM3P in order to prove a consistency between the two models. Section 4 gives summary of the results and the conclusions.

2. Model and experimental design

For this work, aimed to prepare Eta model version for climate-change simulations, we initially adopted the workstation (WS) Eta modeling package (version of 2003) developed at the Science Operations Officer/Science and Training Resource Center (SOO/STRC). This package and its User Guide written by R. Rozumalski is freely available at http://strc.comet.ucar. The SOO/STRC WS Eta is nearly identical to WS Eta model and operational Eta Model of 2003, both developed at NCEP. Only the run-time scripts and model files organization were changed. The additional convection cumulus scheme of Kain and Fritsch (1993) was also implemented. The longest continuous integration with this model can be made for 1 month due to the restriction on the output file name, restart subroutines, and some other impediments.

a. Short description of NCEP Eta model

The full description of the NCEP Eta regional forecasting model is given by Mesinger et al. (1988), Janjic (1994), and Black (1994). In short, the horizontal field structure is described on a semi-staggered E grid. The eta vertical coordinate is used to reduce numerical errors over mountains in computing the pressure gradient force. The planetary boundary layer processes are described by the Mellor-Yamada level 2.5 model (Mellor and Yamada 1974). The convective precipitation scheme is of Betts and Miller (1986) modified by Janjic(1994). The shortwave and longwave radiation codes follow parameterizations of Lacis and Hansen (1974) and Fels and Schwartzkopf (1975), respectively. The land-surface scheme is of Chen et al. (1997). The grid-scale cloud cover fraction is parameterized as a function of relative humidity and cloud water (ice) mixing ratio (Xu and Randall 1996; Hong et al. 1998). Convective cloud cover fraction is parameterized as a function of precipitation rate (Slingo 1987).

b. Modifications in the SOO/STRC WS Eta model

The SOO/STRC WS Eta model has been installed at supercomputer NEC SX6 at CPTEC. To be able to perform long term climate integrations we have made multiple changes and corrections in the scripts and source codes of the original model as well as have written the new programs.

As it was already mentioned, the Eta model was forced at its lateral and bottom boundary by the output of HadAM3P model. The HadAM3P output data represent horizontal wind, potential temperature, specific humidity and earth surface pressure which are given on the horizontal Arakawa B-grid and at the 19 sigma-hybrid levels. These data are written in the PP-format. To use them for the Eta model boundary conditions these data have to be transformed into horizontal wind, geopotential, mixture ratio and earth surface pressure given on regular latitude-longitude grid at standard p-surface levels. For this aim, some of the pre-processing Eta model programs were modified and new program which converts the HadAM3P output data to those acceptable by the Eta model was written.

Another modifications made in the Eta model can be shortly described as following. There were re-written the SST update programs used to accept the SST and SICE data generated by HadCM3 every 15 days. The programs of the Sun's elevation angle and of calendar were modified in order to be able to integrate the Eta model for the artificial year of 360 days which is used by HadAM3P. There were developed new restart programs which can be used in multiprocessing integration. These programs allow to continue the model integration from any time moment by using the model output binary files. This is the useful option for long term climate integration because of the large size of the file of boundary conditions needed for continuous integrations. Another reason for use of the restart option is the large size of the output binary files which after post-processing can be written in more economic GRIB format. All shortcomings which restrict

a period of model integration were corrected including those in the post-processing subroutines.

The additional solar radiation scheme (CLIRAD-SW-M) developed by Chou and Suarez (1999) and modified by Tarasova and Fomin (2000) was implemented in the model. The results of the month integration with this scheme were analysed by Tarasova et al. (2006). The additional thermal radiation scheme of Chou et al. (2001) was also implemented. This allows to run the model with increasing concentration of CO_2 and other trace gases needed for future climate simulation experiments. All these corrections, modifications and implementations were made taking into account that the model can be run on Linux cluster or any other multi-processors computer.

c. Integration with the INPE Eta CCS model

The first step in evaluation of dynamical downscaling results is investigation of a consistency between regional model outputs and GCM data used for RCM boundary conditions. That is, we have to show that our RCM does not significantly diverge from GSM in reproducing time mean large scale patterns of circulation. We also expect that both models reproduce a low-frequency oscillation of the atmosphere in a similar manner.

For this aim we analysed the results of the Eta CCS model integration for the period 1960-1990 over South America. These data are the part of the results of current and future climate downscaling experiments covering the periods of 1960-1990 and 2071-2100, respectively. The detailed analysis of the results of these experiments is currently making by our group and will be present in further publications.

The Eta CCS model in our experiments was forced at its lateral and bottom boundary by the output of HadAM3P, which was run using SST, SICE (sea ice) and greenhouse gases and aerosol concentration as external driving from coupling model HadCM3. Data for lateral boundary conditions for the Eta CCS model were provided every 6 hours and SST and SICE data every

15 days. Linear interpolation for values on lateral boundaries, SST, and SICE was used between these periods. For the initial conditions of soil moisture and soil temperature the climate mean values were used. The spin up period of soil moisture and temperature we have accepted to be equal to 1 year. Hence, the first year of the integration was not used in the analysis.

The area of the integration was centered at 58.5° W longitude and 22.0° S latitude and covers the territory of South American continent with adjacent oceans (55° S - 16° N, 89° W - 29° W). The model was integrated on the 211×115 horizontal grid with grid spacing of 37 km. In the vertical, 38 eta coordinate layers were used. For the modern climate integration the Betts-Miller cumulus convection parametrization scheme and the ETA model original shortwave and longwave radiation schemes were chosen.

3. Analysis of the integration results

The verification of a consistency between the outputs of the Eta CCS model and HadAM3P is particularly important due to the difference between the physical parameterization packages of these two models. To prove an agreement between these models results we have compared the geopotential height, temperature and kinetic energy fields on the earth surface and at the various p-levels (1000 mb, 700 mb, 500 mb) from these two data sources. More detailed comparison was made for the five regions shown in Figure 1: Amazonia (12.5° S - 5° N, 75° W - 48.75° W); Nordeste (north-east of Brazil) (15° S - 2.5° S, 45° W - 33.75° W); South of Brazil (32.5° S - 22.5° S, 60° W - 48.75° W); Minas (22.5° S - 15° S, 48.75° W - 41.25° W); Pantanal (17.5° S - 12.5° S, 60° W - 52.5° W). The time averaged fields and time series of space averaged meteorological variables were analysed.

a. Methods of the analysis

A number of measures of consistency between the outputs of the Eta CCS regional model

(hereafter RM) and HadAM3P global model (hereafter GM) are used here. The original package of programs was developed for comparing the models. First, we assessed the climatological means and time averaged difference between the models, which give an opportunity to identify systematic differences between the models. Then we analysed various characteristics which allow to show in detail a distinction between GM and RM simulated fields. Since this work is dedicated to investigation RM abilities to reproduce mean fields of driving GM and some their statistical moments therefore the regional model fields were scaled to the global model grid. For this aim we removed the small scale component from the regional model fields applying smoothed filter. This filter is the two dimensional version of the weighted moving averages, where the weights depend linearly on the distance between the grid point of the global model and the grid points of the regional model (in which are sited the data used in smoothing procedure). The weight increases when the distance decreases. This smoothing procedure can be written as:

$$\Phi(x_i, y_j) = \sum_{r_{i,j;k} < r_0} \phi(\hat{x}_k, \hat{y}_k)\, p_k \tag{1}$$

where $\Phi(x_i, y_j)$ is a smoothed value of regional model field on global grid point, r_0 is the radius of influence which defines the circle inside which the RM field data are used for average calculation, $r_{i,j;k}$ - the distance from a (x_i, y_j) point of GM grid to k-th RM grid point $(\hat{x}_k, \hat{y}_k)$, $\phi(x_k, y_k)$ are the field value at k-th RM grid point inside the circle defined by the radius of influence, p_k is a weight for the k-th RM grid point and which is calculated as

$$p_k \;=\; \left(1 - \frac{r_{i,j;k}}{r_0}\right) \Big/ \left(\sum_{r_{i,j;k} < r_0} 1 - \frac{1}{r_0} \sum_{r_{i,j;k} < r_0} r_{i,j;k}\right). \tag{2}$$

In this formula the numerator decreases with increasing $r_{i,j;k}$ and becomes equal to zero when $r_{i,j;k}$ is equal or larger than r_0. The denominator is defined from a normalization condition,

namely a sum of all p_k weights must be equal to 1.

In order to compare the models we analysed how they reproduce the time average fields of meteorological variables as well as the fields of standard deviation of these variables. For more detailed assessment of the consistency between the RM and GM fields we also calculated the models' arithmetic difference and coefficients of linear regression using time-series of meteorological variables at each grid point of the Eta model. The fields of these characteristics present useful information about a degree of consistency of the models results.

For quantitative and direct description of the consistency between the RM and GM output fields we propose to use a new characteristic which we termed a consistency index (CI). This characteristic represents some integral variant of Taylor diagram (Taylor, 2001). In terms of correlation coefficient, standard deviations, and mean values of compared fields, it expresses the resemblance of one field to another. It is some simple functional which depends on coefficients of linear regression of one field on another field. We found usefulness of this characteristic in the capability to describe the similarity of two fields by one number only in the case when the space patterns are analysed. The use of unique number for describing the resemblance of two random series is of particular interest in the case when an analysis of consistency of the time evolution of the space patterns is performed. We can analyse in this case the time series of compared fields at every grid point and describe the resemblance of the time evolution of analysed fields by one field only (namely, the consistency index number at every grid point).

The numeric value of CI we define as

$$CI = \begin{cases} (1 - \dfrac{\Delta S_d}{\Delta S_n})\dfrac{\sigma_G}{\sigma_R} & \text{for } \dfrac{\sigma_G}{\sigma_R} \leq 1, \\ (1 - \dfrac{\Delta S_d}{\Delta S_n})\dfrac{\sigma_R}{\sigma_G} & \text{for } \dfrac{\sigma_G}{\sigma_R} > 1. \end{cases} \tag{3}$$

Here σ_G and σ_R are the sample standard deviation of investigated meteorological parameter

of a global model series and a regional model series, respectively. The ΔS_d is the area of figure $ABOCD$ (see Figure 2) which is formed by two straight lines of linear regression and two verticals which intersects them. The straight line r is a linear regression line of the GM series on RM series. The straight line i is an ideal regression line for the identical GM and RM serieses with regression coefficients $a0 = 0$ and $a1 = 1$. The two verticals that intersect these regression lines have the coordinates of $x_R = a - s$ and $x_R = a + s$. The a is a mean value of investigated meteorological parameter of the RM series normalized on $s_0 = 1.44\sigma_R$. The s is a nondimensional value of s_0. The interval ($a - s$, $a + s$) contains 85% of members of the RM series (under the assumption that the series obeys the Gaussian distribution). ΔS_n is the area of a triangle BCE. The area of the shaded figure $ABOCD$ statistically describes a degree of resemblance of the GM and RM serieses: Smaller area corresponds to closer resemblance. The area of the triangle BCE is equal to 2 in nondimensional coordinates and describes the case when the RM and GM serieses are non-correlated and the mean value of the GM series is equal to $a - s$ (or $a + s$). The multiplier $\frac{\sigma_G}{\sigma_R}$ ($\frac{\sigma_R}{\sigma_G}$) approximately describes the ratio of transient-eddy amplitudes reproduced by the models under comparison. Ideally, these amplitudes must be very close. The magnitude of CI is close to 1 if the GM and RM series statistically resemble one another and it is equal to zero or to negative value when there is no similarity of the serieses. When $ABOCD$ is larger than BCE the CI is less than zero what means that the resemblance of the serieses is worse than for the non-correlated serieses with the mean value of the GM series larger (or smaller) than $a + s$ ($a - s$).

Since we had to process very large amount of data, we used recurrence formulas for the calculation of averages, sample standard deviations, and coefficients of linear regression for various GM and RM serieses and wrote these characteristics to the model output every 24 hours. These characteristics for any time period can be recalculated from this running statistics. The

recurrence formulas and formulas that were used for recalculation are presented in appendix A.

b. Assessment of the RM and GM consistency

At first we present geopotential height, temperature and kinetic energy fields averaged over the period of integration from 1961 to 1990. Figures 3 and 4 show these fields at the levels of 1000 mb and 700 mb, respectively, obtained from the RM and GM integrations. A comparison of both models fields at the 1000 mb level shows good agreement between the fields of geopotential height and between the temperature fields. There is general agreement between the kinetic energy fields. Some disagreement in the temperature magnitude exists in the central part of tropical South America. The values of kinetic energy differ over most part of the continent. This is probably related to the different physical parameterization packages in these models. The same RM and GM fields at the higher level of 700 mb bear closer spatial and quantitative resemblance. Note, that the fields similarity at 500 mb (not shown) is higher than that at 700 mb. This is a consequence of the diminishing of the impact of surface-atmosphere interaction on the higher-level atmospheric circulation. We also compared the same RM and GM fields averaged over January and July (not shown). The agreement between the fields is better in July (austral winter) than in January (austral summer). The fields of time standard deviation of meteorological variables provide additional information about an amplitude of their temporal fluctuations. Figure 5 and 6 presents the RM and GM standard deviation fields of geopotential height, temperature and kinetic energy at the 1000 mb and 700 mb levels averaged over the period of integration. One can see reasonably high degree of consistency between the RM and GM standard deviation fields. The standard deviation fields also bear closer resemblance for geopotential height and temperature than for kinetic energy. With the increase of altitude the difference between the RM and GM standard deviation fields is diminished for all variables.

The quantitative distinction between the two fields is usually described by the field of mod-

els' arithmetic difference (MAD) that is the difference between the fields values at each grid point. The left column of Figure 7 shows MAD between the RM and GM geopotential height, temperature, and kinetic energy fields at 1000 mb averaged over the period of integration. One can see that the largest values of this field are seen over the tropical and sub-tropical parts of the Southern American continent. The significant values of MAD over the Andes is probably related to the errors of interpolation from the sigma-hybrid surfaces to the pressure surfaces located below the Earth's surface in the global model. With increasing of the altitude (700 mb, 500 mb) the values of MAD decrease for all fields (Figure 8). The MAD of these variables (geopotential height, temperature, and kinetic energy) averaged over July (January) is smaller (larger) than that averaged over all period of integration.

The right column of Figure 7 presents the consistency index (CI) fields for geopotential height, temperature, and kinetic energy at the level of 1000 mb. The magnitude of CI which is close to 1 means good resemblance between the RM and GM fields. The CI fields resemble the fields of MAD in terms of spatial distribution. But the use of non-dimensional CI allows to compare quantitatively a similarity of the fields of different meteorological variables. Thus, the CI fields in Figure 7 show that the consistency of the fields of geopotential height is higher than that of the temperature fields and the consistency of the kinetic energy field is lower than that of both geopotential height and temperature.

To compare the model outputs we also analysed a temporal variations of the geopotential height, temperature and kinetic energy values at 1000 mb and 500 mb levels, averaged over all integration domain and over the regions shown in Figure 1. Figure 9 presents monthly mean models' arithmetic difference and root mean square difference (RMSD) between the GM and RM time serieses for these variables averaged over the integration domain. For each variable the upper figure represents MAD and the lower figure shows RMSD. One can see that the

magnitude of mean MAD is not high. It is about 6 m in geopotential height, less than 0.1 °K in temperature, and about 10 $m^2\,sec^{-2}$ in kinetic energy at 1000 mb. The mean RMSD values at 1000 mb are not high also. Its magnitude is about 24 m in geopotential heights, 3.4 °K in temperature, and 39 $m^2\,sec^{-2}$ in kinetic energy. Low magnitude of RMSD proves that current absolute values of MAD are not high for each moment of integration. Figure 9 shows also that there is no drift of MAD and RMSD during the integration that proves the RM integration stability. The magnitude of temporal correlation coefficient between the time serieses of the RM and GM space averaged fields is about 0.95-0.98. This means that RM follows the GM boundary driving. At the level of 500 mb as MAD as RMSD are of lower or same magnitude. We also analysed the same time series for the above mentioned regions (Amazonia, Nordeste, South of Brazil, Minas, Pantanal). The correlation coefficients between the RM and GM time serieses as well as mean MAD and RMSD at 1000 mb and 500 mb are shown in Table 1 for all domain and for the five regions. One can see that these coefficients slightly varies from region to region. Note one case of low correlation between the kinetic energy time series at 1000 mb in Amazonia related to low magnitude of wind at the surface level in GM.

Figures 10 and 11 show the time evolution of annual mean MAD in the geopotential height, temperature and kinetic energy fields at 1000 mb and 700 mb, respectively, for the above mentioned regions. At the 1000 mb level the magnitude of MAD for different regions varies from -10 m to +17 m for geopotential height, from -4.0°K to +0.3°K for temperature, and from -20 $m^2\,sec^{-1}$ to -5 $m^2\,sec^{-1}$ for kinetic energy. The amplitude of interannual variations of these meteorological variables differs from one region to another. We can see that there is no significant trend and strong fluctuations of MAD for any region. A significant mutual correlation between the MAD obtained for various regions does not exist. Note that the values of MAD and the amplitudes of its interannual variations for geopotential height and temperature decrease when

the altitude increases. For kinetic energy both MAD and amplitude of interannual variations increase when the altitude increases. Though the magnitude of relative MAD (for example, that divided by a mean standard deviation) for kinetic energy also decreases.

Figure 12 presents a scattering diagram of daily linear regression coefficients values (a0, a1) which describe the regression of the GM 1000 mb geopotential height field on the same RM field (top); time evolution of these linear regression coefficients (a0 , a1) (middle) for each month of the model run; and the time evolution of consistency index (bottom). The consistency index was calculated in the same way as described above (Figure 2), but the time series were substituted by "space" series formed by variable values at all grid points.

Concerning this figure we can say that in the hypothetical case, when the fields of GM and RM coincide, all points in the top figure will fall on one point with the coordinates a1=1.0 and a0=0.0. Thus we can affirm that if the points on the top figure are located near the point (a1=1, a0=0) the RM and GM fields are very similar; in the case when the points are reasonably scattered but the center of mass of this distribution is close to the point (a1=1, a0=0) we can say that the fields of the models are similar in average. The time series of linear regression coefficients a0 and a1 of GM data upon RM data have large negative correlation (middle figure). In the most cases it leads to some compensation in the variations of CI shown on the bottom figure. The CI variations clearly express the year oscillation. Its mean value is about 0.94 and increases with the altitude. Its linear time trend is very small. This provides some more indication that the considered models do not diverge. Figure 13 presents the same characteristics as shown in Figure 12 but for the RM and GM temperature fields at 1000 mb. The scattering diagrams in this case indicates that GM is slightly warmer then RM for the regions with low temperatures and slightly colder for the regions with higher temperatures. This is in agreement with Figure 3 which shows mean temperature fields for all period of the integration.

For more detailed analysis of the time evolution of mean values of meteorological variable fields we have calculated spectral distribution of their time series by using Fast Fourier Transform algorithm. Figure 14 shows an example of such distribution for the time series of geopotential height, temperature and kinetic energy averaged over all integration domain. One can see that the GM and RM spectras have a high degree of similarity. The high frequency tails quasi coincide. The year and semi-year oscillations have the same amplitude. Four year cycle in geopotential height and temperature is reproduced by RM and GM quasi identically. This cycle in kinetic energy spectra is also reproduced by both models but not identically. Also the models agree in reproducing of 6-9 years minimum and of the next increase of the spectra. Quasi all synoptic and seasonal oscillation maximums coincide in the RM and GM spectras. We calculated the same spectras for above mentioned regions shown in Figure 1. The RM and GM spectras for these regions demonstrate similar coincidence as that for all integration domain with insignificant distinctions. Only for the Pantanal region, the spectras of GM and RM kinetic energy at 1000 mb diverge significantly. But with the increase of altitude this difference diminishes and quasi disappears at 500 mb.

4. Conclusions

This analysis of the output results of 30-year runs of regional model and its driving global model confirms that the models have a high degree of consistency despite of the difference in their physical parameterizations. In the future work we are planning to estimate an impact of tuning in RM physical parameterizations such as radiation and convection schemes on consistency of RM and GM output fields. An impact of the use of another driven global model on the RM and GM resemblance will be also estimated. We also need to evaluate the model performance for current climate by comparing regional model outputs with observations on global and regional scales. In order to estimate the impact of global model errors on the regional

model outputs, the integration of the regional model driven by the reanalysis data (Kanamitsu et al. 2002) is planned. The approach developed in this paper can form the basis for quantitative assessment of regional model and its driving global model consistency. Currently, many researchers use various regional models for dynamical downscaling but a few publications exist about the quantitative assessment of the similarity between the large-scale fields of a regional model and its driving global model. Even if regional and global models have the same physical parameterization packages, the difference between the models can be related to the low time frequency and low space resolution of boundary forcing in the regional model.

Appendix A *Recurrence formulas*

For the evaluation of the consistency of the models we analysed very large serieses of the meteorological data. To make the work with series faster and for economy of computer resources we used recurrence formulas for calculating running average, standard deviation and covariance, from which we can calculate any others necessary characteristics.

We accept the definition of running mean, variance and covariance respectively as

$$\bar{x}_n = \frac{1}{n}\sum_{i=1}^{n} x_i, \tag{A1}$$

$$D_n = \frac{1}{n}\sum_{i=1}^{n}(x_i - \bar{x}_n)^2, \tag{A2}$$

$$r_n = \frac{1}{n}\sum_{i=1}^{n}(x_i - \bar{x}_n)(y_i - \bar{y}_n). \tag{A3}$$

Here $\bar{x}_n$, D_n, and r_n are the sample mean, the sample variance, and the sample covariance for serieses containing n terms, x_i, y_i are the i-th term of series. The recurrence formula for a sample mean is obvious

$$\bar{x}_n \;=\; \frac{n-1}{n}\bar{x}_{n-1} + \frac{1}{n}x_n. \tag{A4}$$

Below we derive the recurrence formula for a sample covariance. The analogous formula for a sample variance is obtained after replacing y_i, $\bar{y}_n$ by x_i, $\bar{x}_n$.

Let us rewrite formula (A3) using (A4) in following manner

$$r_n \;=\; \frac{n-1}{n}\cdot\frac{1}{n-1}\sum_{i=1}^{n-1}(x_i - \frac{n-1}{n}\bar{x}_{n-1} - \frac{1}{n}x_n)(y_i - \frac{n-1}{n}\bar{y}_{n-1} - \frac{1}{n}y_n) +$$

$$+\frac{1}{n}(x_n - \bar{x}_n)(y_n - \bar{y}_n)$$

Now we group the members of this formula to select the part that is equal to the covariance on previous $(n-1)$ step

$$r_n \;=\; \frac{n-1}{n}\cdot\frac{1}{n-1}\sum_{i=1}^{n-1}(x_i - \bar{x}_{n-1})(y_i - \bar{y}_{n-1}) + \frac{1}{n}(\bar{y}_{n-1} - y_n)\cdot\frac{n-1}{n}\cdot\frac{1}{n-1}\sum_{i=1}^{n-1}(x_i -$$

$$-\bar{x}_{n-1}) + \frac{1}{n}(\bar{x}_{n-1} - x_n)\frac{n-1}{n}\cdot\frac{1}{n-1}\sum_{i=1}^{n-1}(y_i - \bar{y}_{n-1}) + \frac{1}{n}(\bar{x}_{n-1} - x_n)\cdot\frac{1}{n}(\bar{y}_{n-1} - y_n)\cdot$$

$$\cdot\frac{n-1}{n} + \frac{1}{n}(x_n - \bar{x}_n)(y_n - \bar{y}_n).$$

Taking into account that the terms $\frac{1}{n-1}\sum_{i=1}^{n-1}(x_i - \bar{x}_{n-1})$ and $\frac{1}{n-1}\sum_{i=1}^{n-1}(y_i - \bar{y}_{n-1})$ are equal to zero and using again formula (A4) we obtain

$$r_n \;=\; \frac{n-1}{n}r_{n-1} + \frac{n-1}{n^2}(\bar{x}_{n-1} - x_n)(\bar{y}_{n-1} - y_n). \tag{A5}$$

Finally we show how to recalculate these running values for any time interval. Let $\bar{x}_m$ be the mean value for series from the first m elements of x_i and let $m < n$. Denote $\bar{x}_{m:n}$ the mean value of x_i for the series $x_{m+1}, x_{m+2}, ...x_n$ as

$$\bar{x}_{m:n} \;=\; \frac{1}{n-m}\sum_{i=m+1}^{n} x_i,$$

It is easy to obtain that

$$\bar{x}_{m:n} \;=\; \frac{1}{n-m}(n\bar{x}_n - m\bar{x}_m). \tag{A6}$$

Now, let us derive formula for calculating the covariance for interval $(m+1, n)$ using the meanings for covariance and average for intervals $(1, m)$ and $(1, n)$.

$$n\bar{r}_n - m\bar{r}_m = \sum_{i=1}^{n}(x_i y_i) - n\bar{x}_n\bar{y}_n - \sum_{i=1}^{m}(x_i y_i) + m\bar{x}_m\bar{y}_m \tag{A7}$$

Taking into account that

$$(n-m)\bar{r}_{m:n} = \sum_{i=m+1}^{n}(x_i y_i) - (n-m)\bar{x}_{m:n}\bar{y}_{m:n}, \tag{A8}$$

we rewrite (A7) as

$$n\bar{r}_n - m\bar{r}_m = (n-m)\bar{r}_{m:n} - n\bar{x}_n\bar{y}_n + m\bar{x}_m\bar{y}_m + (n-m)\bar{x}_{m:n}\bar{y}_{m:n}. \tag{A9}$$

Lastly, substituting the $\bar{x}_{m:n}, \bar{y}_{m:n}$ from formula (A6) and making routine transformations we obtain the desired formula

$$\bar{r}_{m:n} = \frac{1}{n-m}(n\bar{r}_n - m\bar{r}_m) - \frac{mn}{(n-m)^2}(\bar{x}_n - \bar{x}_m)(\bar{y}_n - \bar{y}_m). \tag{A10}$$

Acknowledgments. I.A. Pisnichenko was supported by Global Opportunity Fund (GOF) from UK Foreign Commonwealth Office, T.A. Tarasova was sponsored by INPE/CPTEC as part of an international agreement with the NEC Corporation. The authors thank their colleagues from CPTEC/INPE C. Nobre and J. Marengo for their administrative contributions that made it possible for us to perform this work. The authors also thank Hadley Center for presenting HadAM3P data.

References

Betts AK, and Miller MT (1986) A new convective adjustment scheme. Part II: Single column tests GATE wave, BOMEX, and Arctic air-mass data. Quart J Roy Met Soc 112: 693-703

Black TL (1994) NMC notes: the new NMC mesoscale Eta model: description and forecast examples. Wea Forecasting 9:256-278

Castro CL, Pielke Sr RA, and Leoncini G (2005) Dynamical downscaling: Assessment of value retained and adding using the Regional Atmosphering Modeling System (RAMS). J Geophys Res 110(D05108) doi: 10.1029/2004JD004721

Chou M-D, and Suarez MJ (1999) A solar radiation parameterization (CLIRAD-SW) for atmospheric studies. Preprint NASA/Goddard Space Flight Center, Greenbelt, Maryland, 38 pp

Chou M-D, Suarez MJ, Liang X-Z, and Yan M M-H (2001) A thermal infrared radiation parameterization for atmospheric Studies. Preprint NASA/Goddard Space Flight Center, Greenbelt, Maryland, 55 pp

Chen FK, Janjic Z, and Mitchel K, (1997) Impact of the atmospheric surface-layer parameterizations in the new land-surface scheme of the NCEP mesoscale Eta model. Bound-Layer Meteor 85: 391-421

Christensen JH, Carter T, and Giorgi F (2002) PRUDENCE employs new methods to assess European climate change. EOS Trans Amer Geophys Union 82:147

Chou SC, Nunes AMB, and Cavalcanti IFA (2000) Extended forecast over South America using the regional Eta model. J Geophys Res 105:10147-10160.

Chou SC, Tanajura CAS, Xue Y, and Nobre CA (2002) Validation of the coupled Eta/SSiB model over South America. J Geophys Res 107:8088 doi:10.1029/2000JD000270

Duffy PB, Arritt RW, Coquard J, Gutowski W, Han J, Iorio J, Kim J, Leung L-R, Roads J, Zeledon E (2006) Simulations of present and future climates in the western United States with four nested

regional climate models. J Clim 19:873-895

Dickinson RE, Errico RM, Giorgi F, and Bates GT (1989) A regional climate model for the western United States. Clim Change 15:383-422

Fels SB, and Schwartzkopf MD (1975) The simplified exchange approximation: A new method for radiative transfer calculations. J Atmos Sci 32:1475-1466

Fernandez JPR, Franchito SH, and Rao VB (2006) Simulation of the summer circulation over South America by two regional climate models. Part I: Mean climatology. Theor Appl Climatol 86:247-260

Figueroa SN, Satyamurty P, and de Silva Dias PL (1995) Simulations of the summer circulation over the South American region with the Eta coordinate model. J Atmos Sci 52:1573-1584

Giorgi F, and Bates GT (1989) The climatological skill of a regional model over complex terrain. Mon Wea Rev 117:2325-2347

Giorgi F, Bi X, Pal JS (2004) Mean, interannual variability and trends in a regional climate change experiment over Europe. I. Present-day climate (1961-1990). Clim Dyn 22:733-756 doi: 10.1007/s00382-004-0409-x

Hong S-Y, Yuang H-M, and Zhao Q (1998) Implementing of prognostic cloud scheme for a regional spectral model. Mon Wea Rev 126:2621-2639

Hudson DA, and Jones RD (2002) Regional climate model simulations of present-day and future climates of Southern Africa. Hadley Centre for Climate Prediction and Research, Met Office, Bracknell, UK

Janjic ZI (1994) The step-mountain eta coordinate model: further development of the convection, viscous sublayer, and turbulence closure schemes. Mon Wea Rev 122:927-945

Jones RG, Murphy JM, Noguer M, Keen AB (1997) Simulation of climate change over Europe using a nested regional-climate model. II: Comparison of driving and regional model responses

to a doubling of carbon dioxide. Quart J Roy Met Soc 123:265-292

Jones RG, Noguer M, Hassel DC, Hudson D, Wilson SS, Jenkins GJ, and Mitchell JFB (2004) Generating high resolution climate change scenarios using PRECIS. Met Office, Hadley Center, Exeter, UK, 40 pp

Kanamitsu M, Ebisuzaki W, Woollen J, Yang S-K, Hnilo JJ, Fiorino M, and Potter GL (2002) NCEP-DOE AMIP-II Reanalysis (R-2). Bull Amer Meteor Soc 83:1631-1643

Kain JS, and Fritsch JM (1993) A one-dimensional entraining detraining plume model and its applications in convective parameterization. J Atmos Sci 23:2784-2802

Lacis AA, and Hansen JE (1974) A parameterization for the absorption of solar radiation in the Earth's atmosphere. J Atmos Sci 31:118-133

Laprise R, Caya D, Frigon A, Paquin D (2003) Current and perturbed climate as simulated by the second-generation Canadian Regional Climate Model (CRCM-II) over north-western North America. Clim Dyn 21:405-421 doi: 10.1007/s00382-003-0342-4

Laprise R (2006) Regional climate modelling. J Comput Phys doi: 10.1016/j.jcp.2006.10.024

Laprise R, de Elia R, Caya D et al (2007) Challenging some tenets of regional climate modelling.

Mellor GL, and Yamada T (1974) A hierarchy of turbulence closure models for boundary layers. J Atmos Sci 31:1791-1806.

Mesinger F, Janjic ZI, Nickovic S, Gavrilov D, and Deaven DG (1988) The step-mountain coordinate: model description and performance for cases of Alpine lee cyclogenesis and for a case of Appalachian redevelopment. Mon Wea Rev 116:1493-1518

Roeckner E, Aroe K, Bengtsson L et al (1996) The atmospheric general circulation model ECHAM-4: model description and simulation of present day climate. Technical report, 218, Max-Plank Institute for Meteorology

Pal JS, Giorgi F, Bi X et al (2006) The ICTP RegCM3 and RegCNET: regional climate modeling

for the developing World. Bull Am Meteorol Soc (in press)

Pielke Sr RA et al (1992) A comprehensive meteorological modeling system - RAMS. Meteorol Atmos Phys 49:69-91

Pisnichenko IA, Tarasova TA, Fernandez JPR, and Marengo J (2006) Validation of the Eta WS regional climate model driven by boundary conditions from the HADAM3P over South America. Proceedings of 8 ICSHMO, Foz do Iguacu, Brazil, April 24-28, INPE, 595-597

Seth A, Rauscher SA, Camargo SJ (2007) RegCM3 regional climatologies for South America using reanalysis and ECHAM global model driving fields. Clim Dyn 28:461-480 doi: 10.1007/s00382-006-0191-z

Slingo JM (1987) The development of a cloud prediction model for the ECMWF model. Quart J Royal Met Soc 113:899-927

Tanajura CAS (1996) Modeling and analysis of the South American summer climate. PhD Thesis, Univ of Md, College Park, 164 pp

Tarasova TA, and Fomin BA (2000) Solar radiation absorption due to water vapor: Advanced broadband parameterizations. J Appl Meteor 39:1947-1951

Taylor KE (2001) Summarizing multiple aspects of model performance in single diagram: J Geophys Res 106:7183-7192

Vernekar AD, Kirtman BP, Fennessy MJ (2003) Low-level jets and their effects on the South American summer climate by the NCEP Eta Model. J Clim 16:297-311

Tarasova TA, Fernandez JPR, Pisnichenko IA, Marengo JA, Ceballos JC, and Bottino MJ (2006) Impact of new solar radiation parameterization in the Eta Model on the simulation of summer climate over South America. J Appl Meteor Climatol 44:318-333

Wang Y, Leung LR, McGregor JL, Lee D-K, Wang W-C, Ding Y, and Kimura F (2004) Regional climate modeling: progress, challenges, and prospects. J Meteor Soc Jpn 82:1599-1628

Xu K-M, and Randall DA (1996) A semi empirical cloudiness parameterization for use in climate models. J Atmos Sci 53:3084-3102

Figure captions

Figure 1. The regions over South America selected for the analysis: Amazonia (1), Nordeste (2), Sul Brasil (3), Minas (4), Pantanal (5).

Figure 2. Definition of consistency index by using the coefficients of linear regression of HadAM3P field on Eta CCS model field.

Figure 3. Mean (1961-1990) fields of geopotential height (m), temperature (°K), and kinetic energy ($m^2\,sec^{-2}$) at 1000 mb, provided by HadAM3P (left) and Eta CCS model (right) simulations.

Figure 4. The same as in Figure 2 but at 700 mb.

Figure 5. Mean (1961-1990) standard deviation fields of geopotential height (m), temperature (°K), and kinetic energy ($m^2\,sec^{-2}$) at 1000 mb, provided by HadAM3P (left) and Eta CCS model (right) simulations.

Figure 6. The same as in Figure 4 but at 700 mb.

Figure 7. Mean (1961-1990) fields of MAD (left), calculated for HadAM3P and Eta CCS model fields of geopotential height (m), temperature (°K), and kinetic energy ($m^2\,sec^{-2}$) at 1000 mb, and consistency index between HadAM3P and Eta CCS model(right), calculated for the same fields.

Figure 8. The same as in Figure 7 but at 700 mb.

Figure 9. Time series of mean (over the integration domain) MAD and RMSD, calculated for HadAM3P and Eta CCS model fields of geopotential height (m), temperature (°K), and kinetic energy ($m^2\,sec^{-2}$) at 1000 mb (left) and 500 mb (right).

Figure 10. Time series of mean (over the regions shown in Figure 1) MAD, calculated for HadAM3P and Eta CCS model fields of geopotential height, G (m), temperature, T (°K), and kinetic energy, KE ($m^2\,sec^{-2}$) at 1000 mb.

Figure 11. The same as in Figure 10 but at 700 mb.

Figure 12. Scattering diagram of daily coefficients (a0, a1) of linear regression of HadAM3P field on Eta CCS model field of geopotential height at 1000 mb calculated over the all integration domain (top); time series of regression coefficients (a0, a1) (middle), time series of consistency index for these models (bottom).

Figure 13. The same as in Figure 12 but for temperature at 1000 mb.

Figure 14. Time spectra of mean (over the integration domain) geopotential height (top), temperature (middle), and kinetic energy (bottom) at 1000 mb, provided by HadAM3P (solid) and Eta CCS model (dot-dashed) simulations.

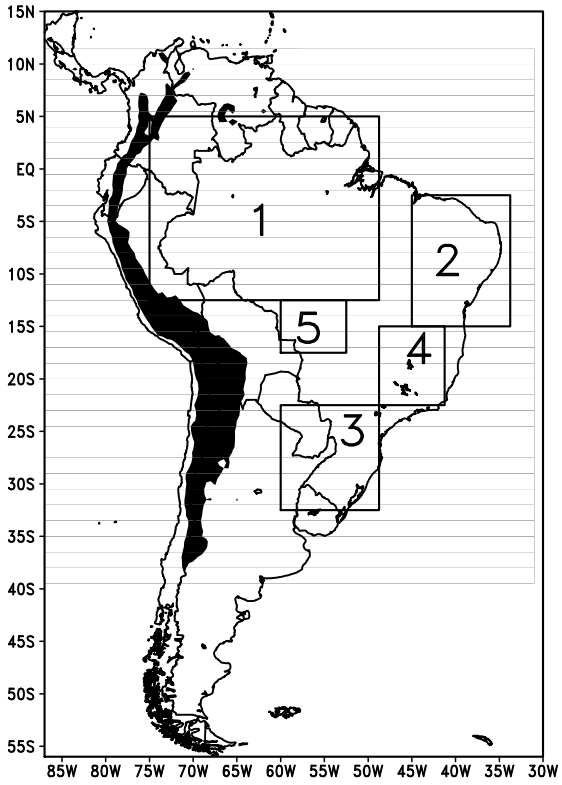

Figure 1: The regions over South America selected for the analysis: Amazonia (1), Nordeste (2), Sul Brasil (3), Minas (4), Pantanal (5).

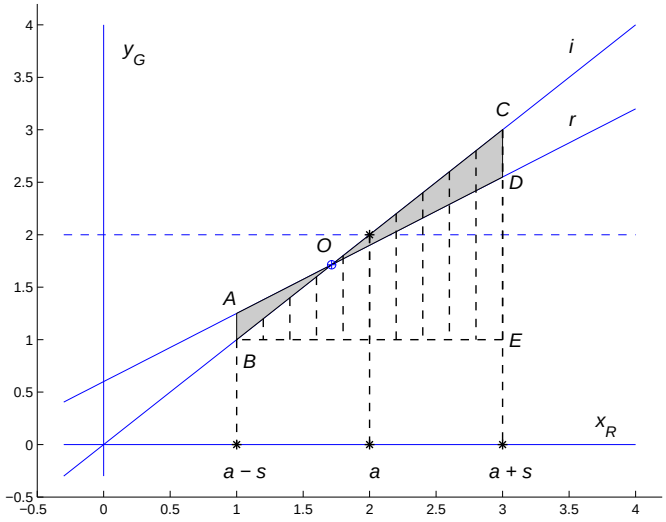

Figure 2: Definition of consistency index by using the coefficients of linear regression of HadAM3P field on Eta CCS model field.

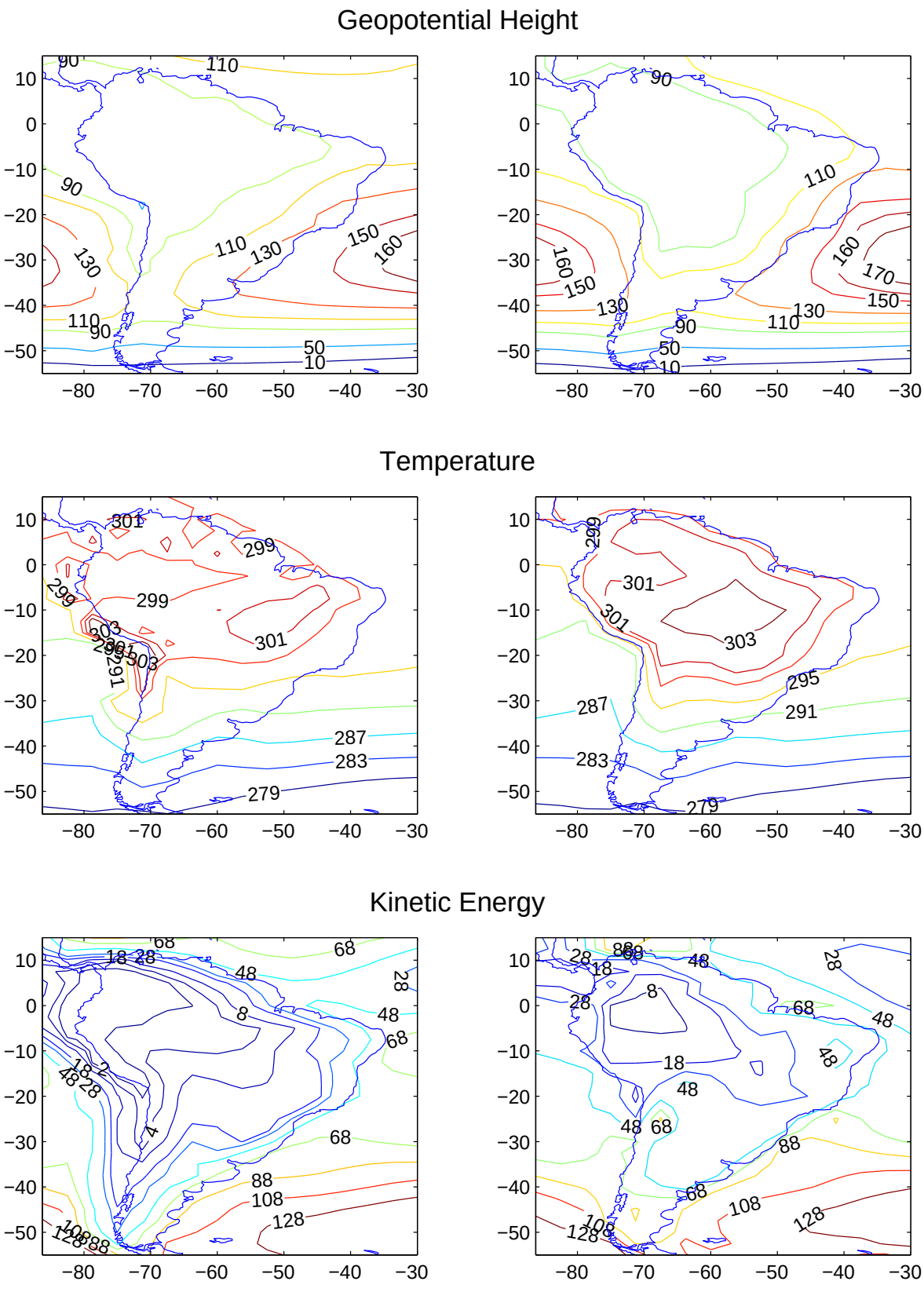

Figure 3: Mean (1961-1990) fields of geopotential height(m), temperature (°K), and kinetic energy ($m^2\,sec^{-2}$) at 1000 mb, provided by HadAM3P (left) and Eta CCS model (right) simulations.

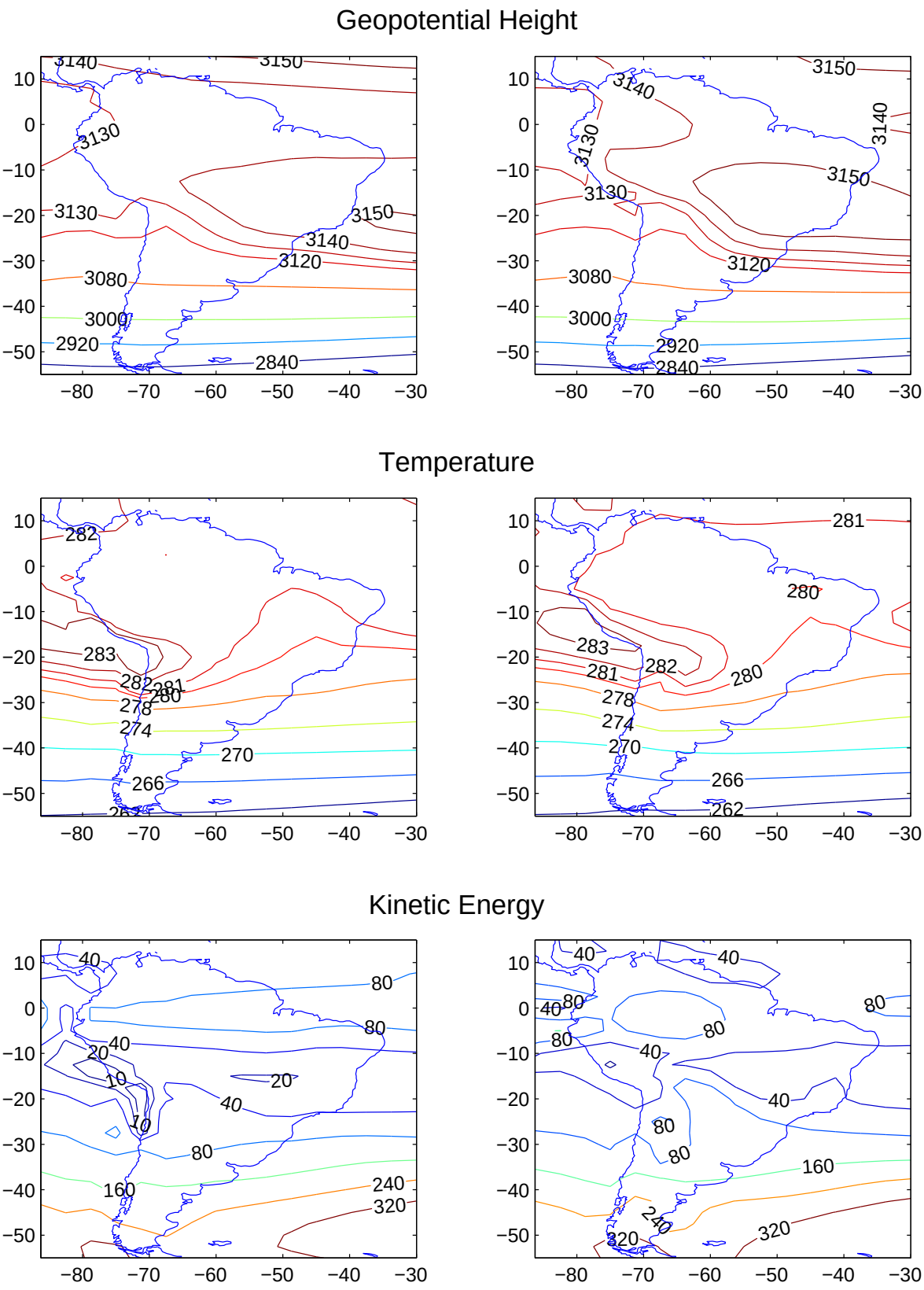

Figure 4: The same as in Figure 2 but at 700 mb.

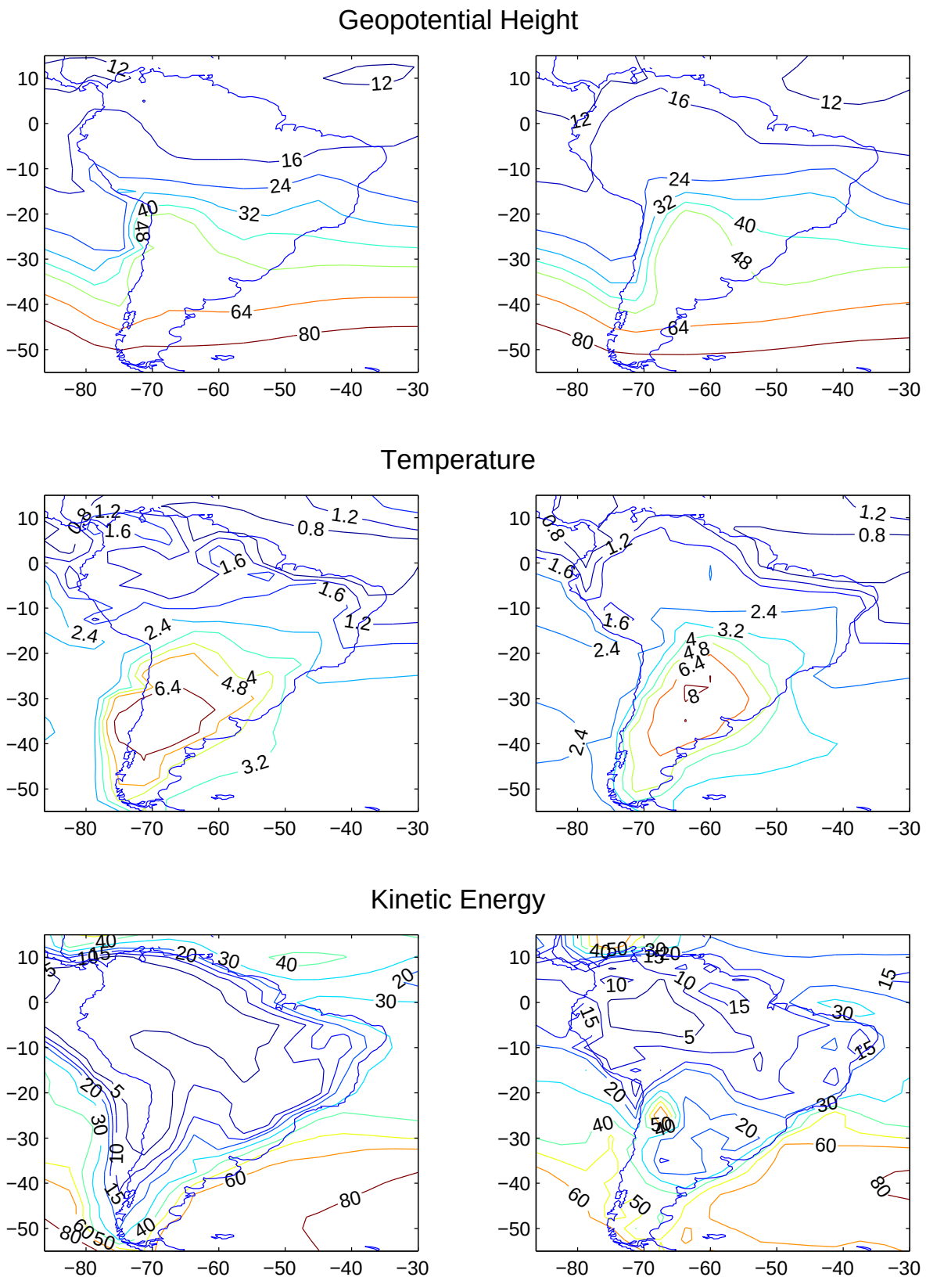

Figure 5: Mean (1961-1990) standard deviation fields of geopotential height (m), temperature (°K), and kinetic energy ($m^2\,sec^{-2}$) at 1000 mb, provided by HadAM3P (left) and Eta CCS model (right) simulations.

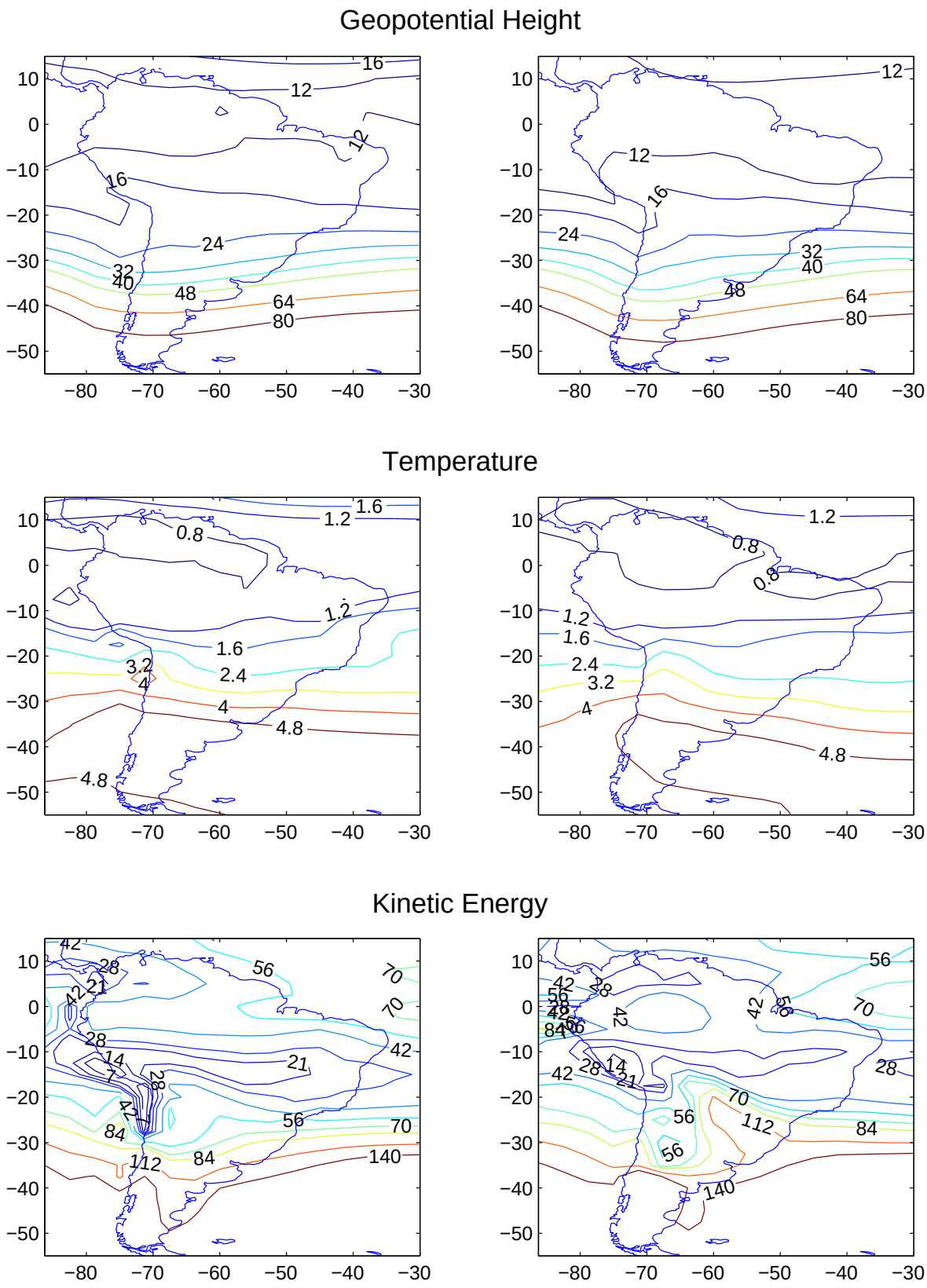

Figure 6: The same as in Figure 4 but at 700 mb.

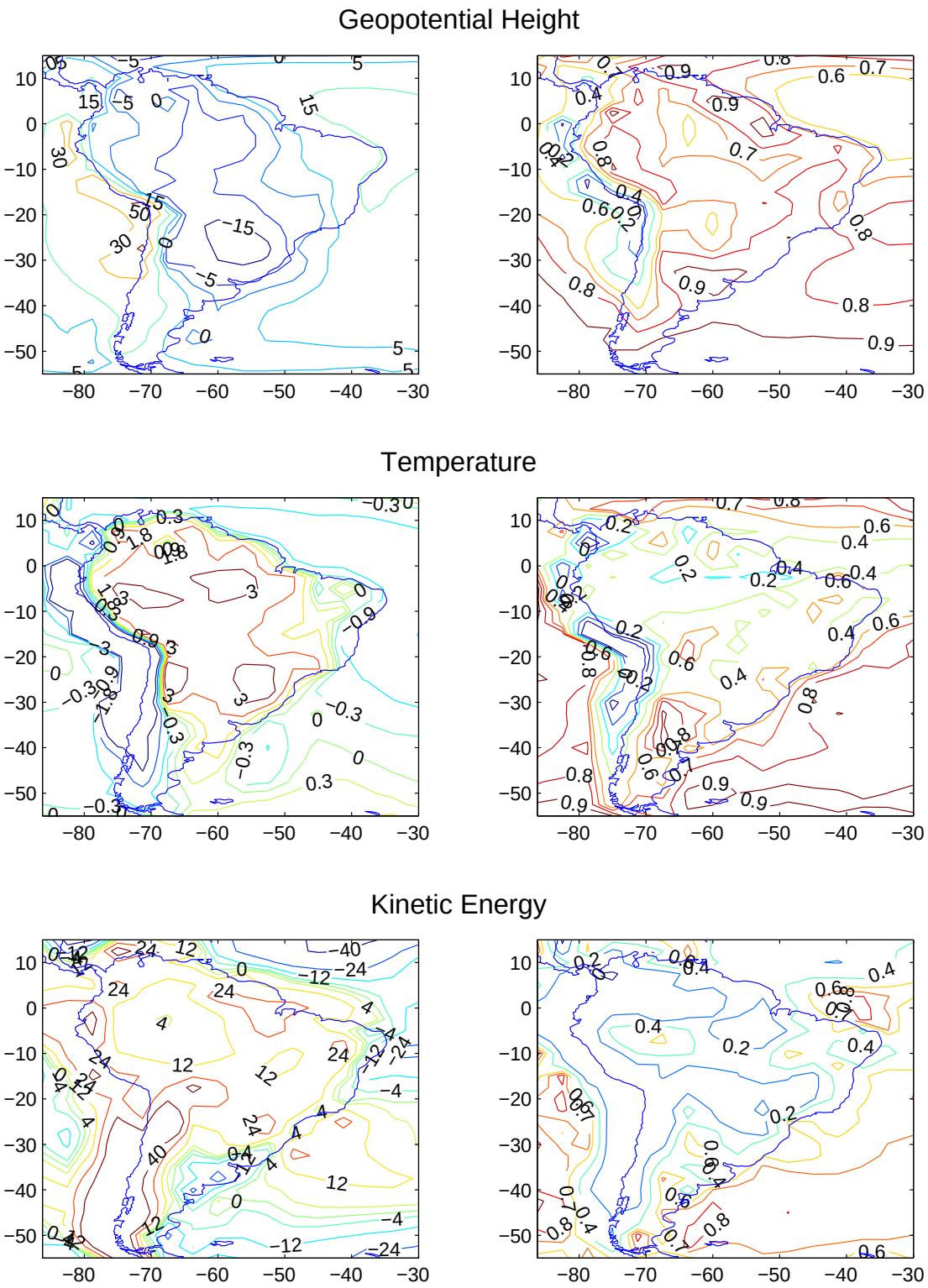

Figure 7: Mean (1961-1990) fields of MAD (left), calculated for HadAM3P and Eta CCS model fields of geopotential height (m), temperature (°K), and kinetic energy ($m^2\,sec^{-2}$) at 1000 mb, and consistency index between HadAM3P and Eta CCS model(right), calculated for the same fields.

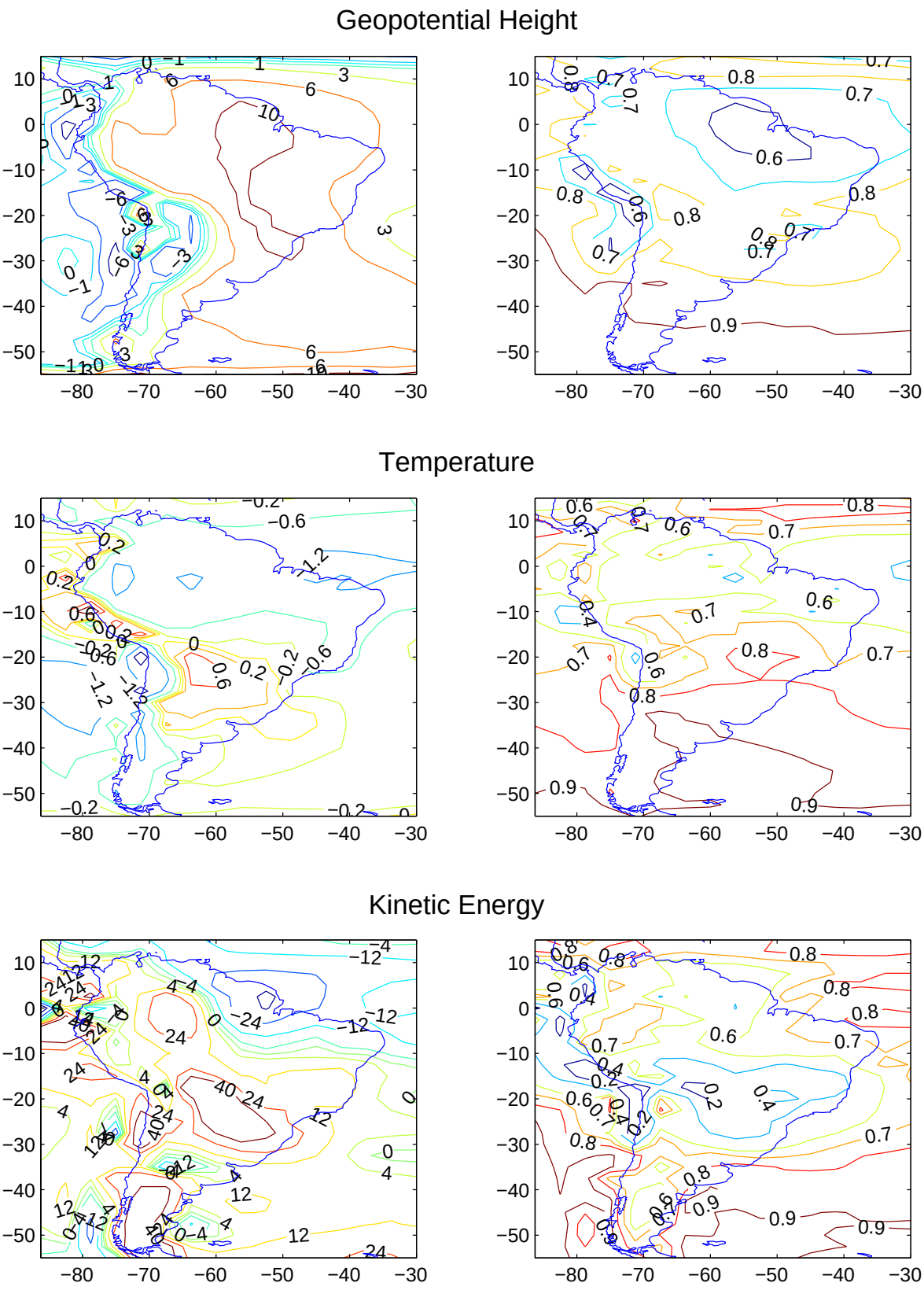

Figure 8: The same as in Figure 7 but at 700 mb.

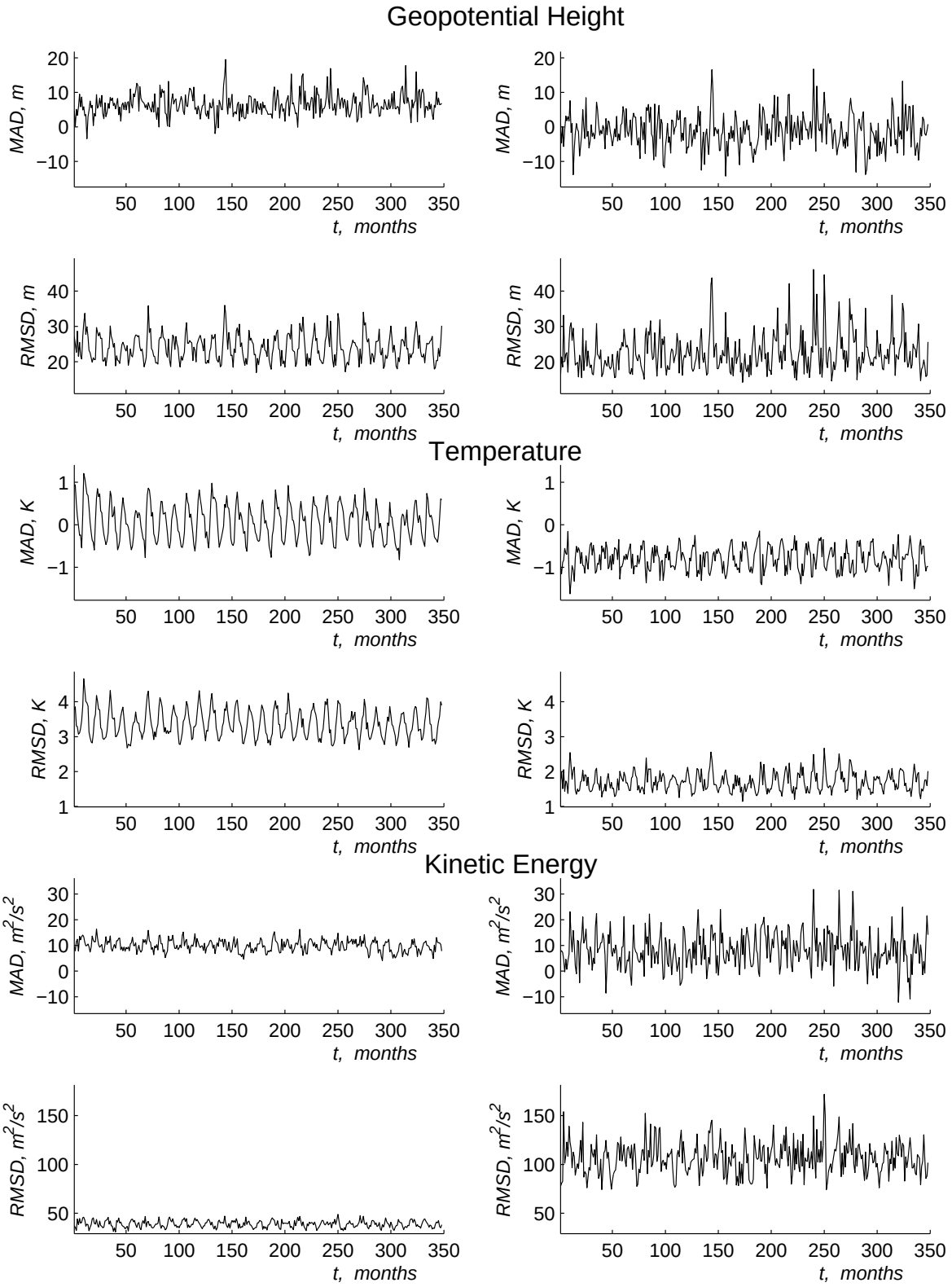

Figure 9: Time series of mean (over the integration domain) MAD and RMSD, calculated for HadAM3P and Eta CCS model fields of geopotential height (m), temperature (°K), and kinetic energy ($m^2\,sec^{-2}$) at 1000 mb (left) and 500 mb (right).

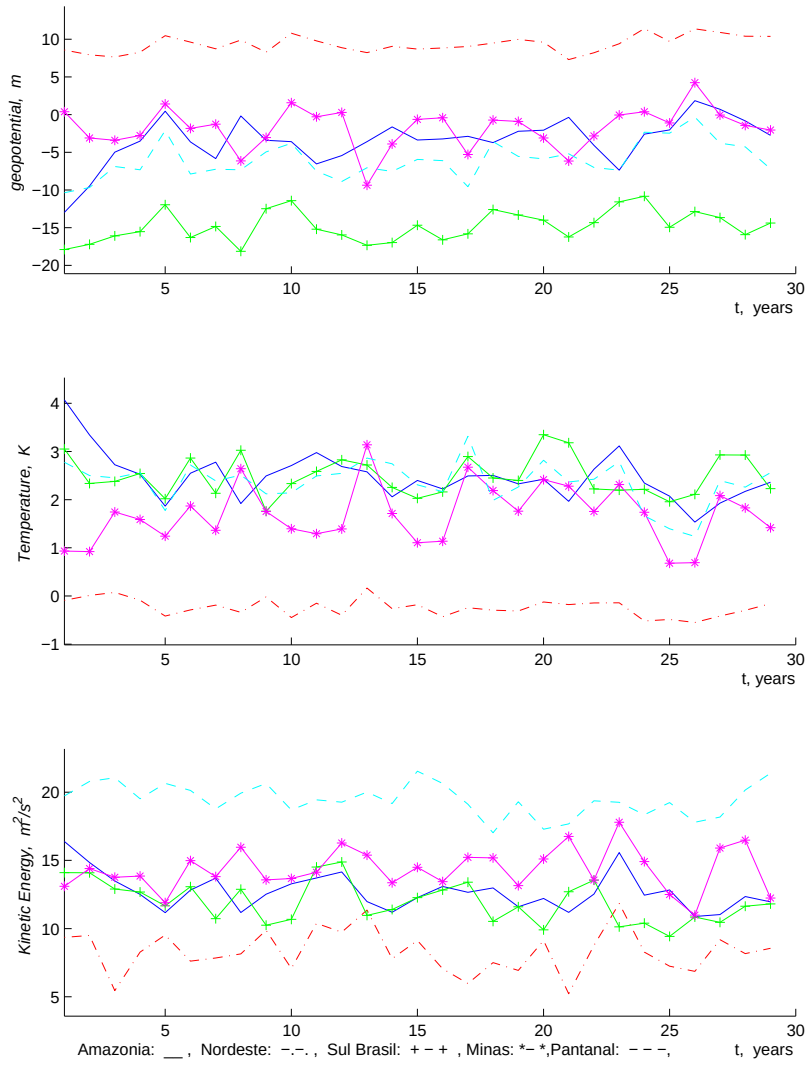

Figure 10: Time series of mean (over the regions shown in Figure 1) MAD, calculated for HadAM3P and Eta CCS model fields of geopotential height, G (m), temperature, T (°K), and kinetic energy, KE ($m^2\,sec^{-2}$) at 1000 mb.

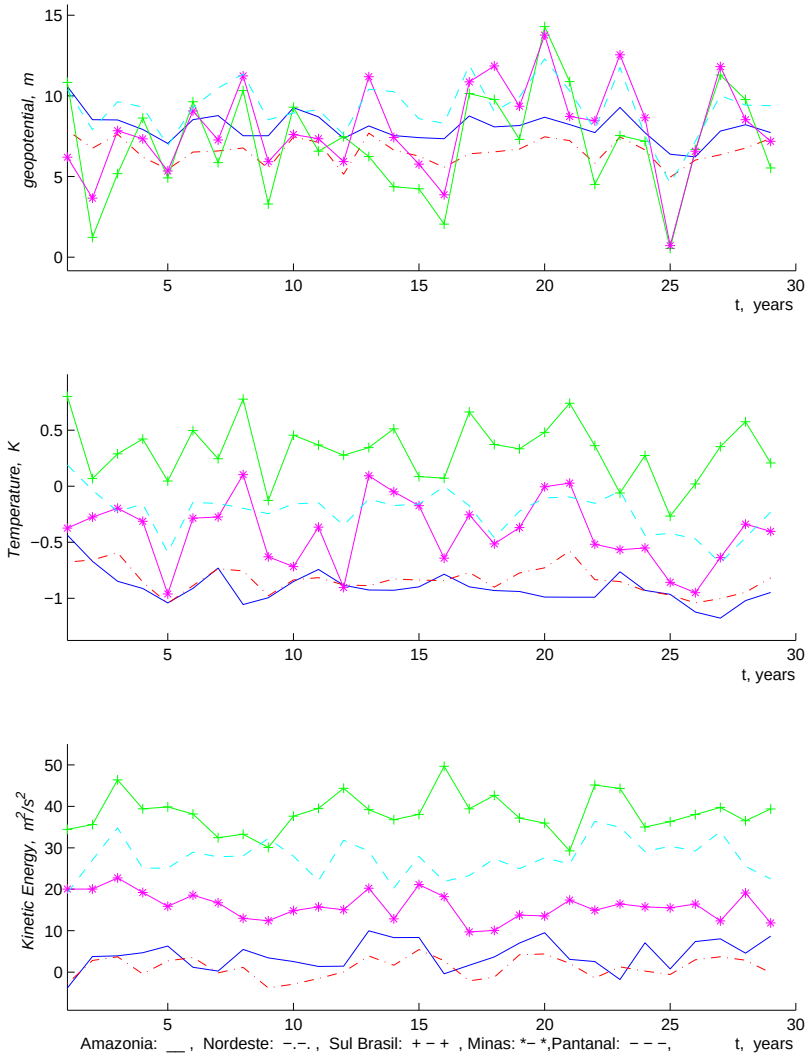

Figure 11: The same as in Figure 10 but at 700 mb.

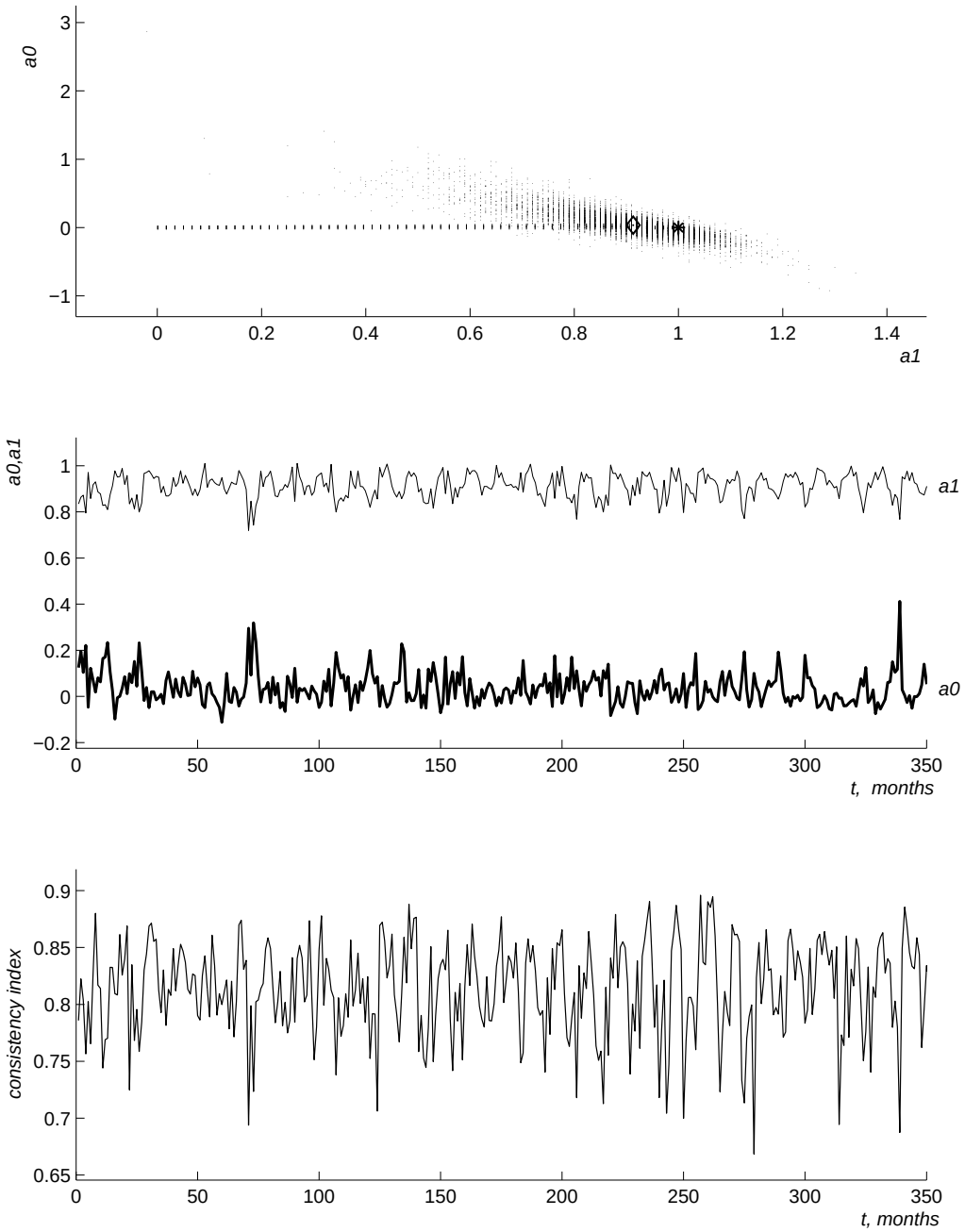

Figure 12: Scattering diagram of daily coefficients (a0, a1) of linear regression of HadAM3P field on Eta CCS model field of geopotential height at 1000 mb calculated over the all integration domain (top); time series of regression coefficients (a0, a1) (middle), time series of consistency index for these models (bottom).

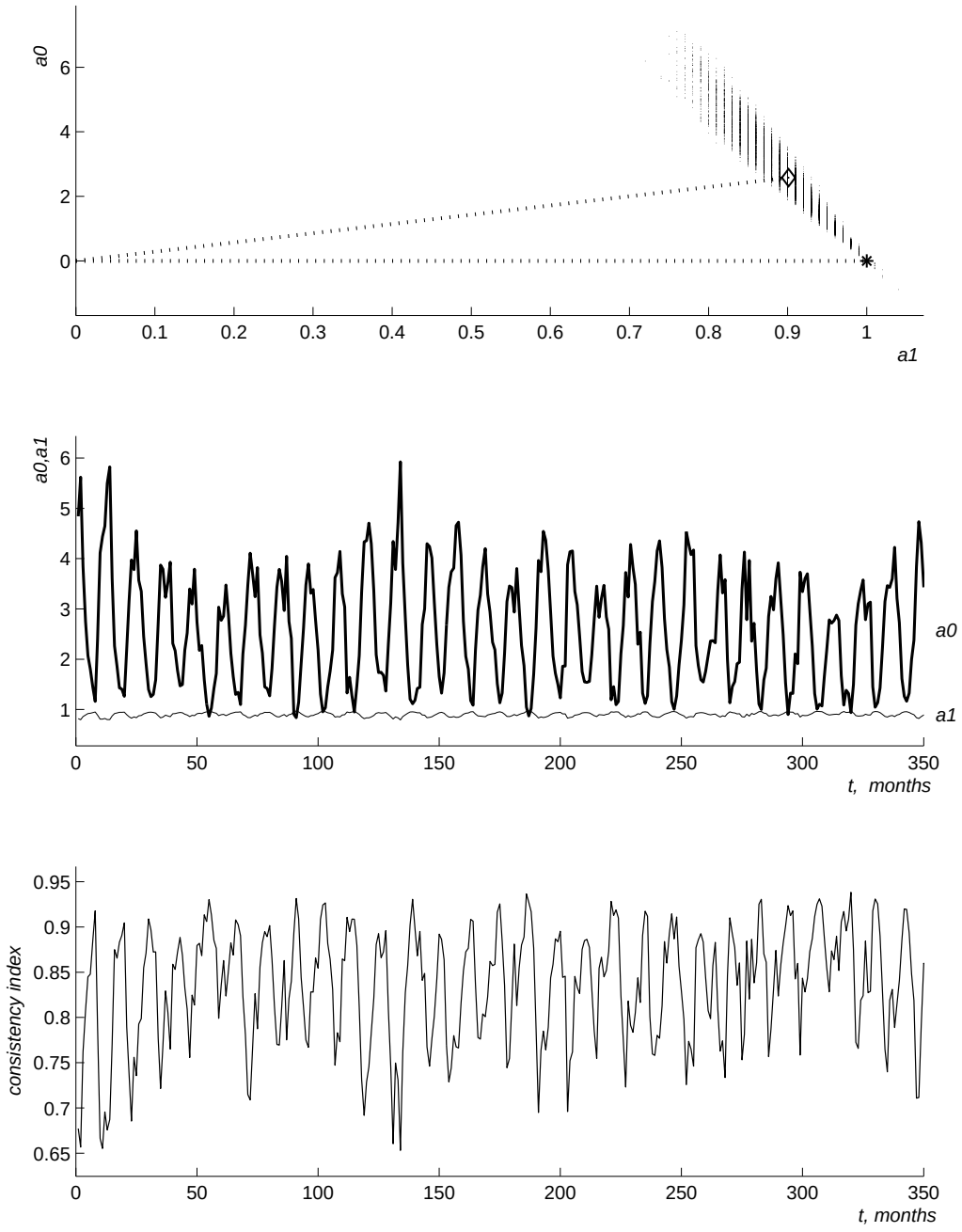

Figure 13: The same as in Figure 12 but for temperature at 1000 mb.

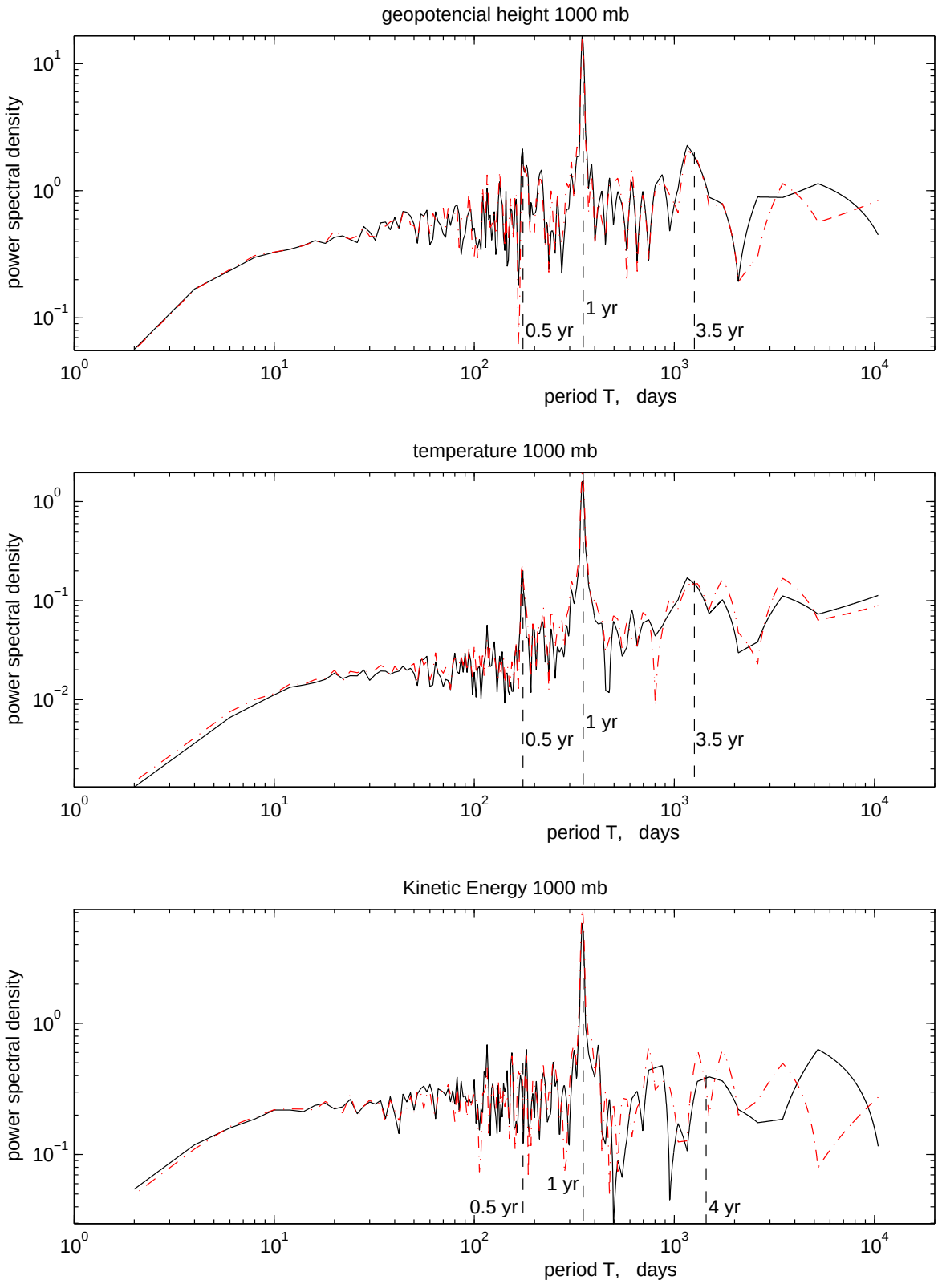

Figure 14: Time spectra of mean (over the integration domain) geopotential height (top), temperature(middle), and kinetic energy (bottom) at 1000 mb, provided by HadAM3P (solid) and Eta CCS model (dot-dashed) simulations.

Table 1. Mean correlation coefficient (r), mean MAD , and mean RMSD between the regional and global models time series of geopotential height (G), temperature (T), and kinetic energy (KE) at 1000 mb and 500 mb, averaged over the integration domain (D) and over the 5 regions shown in Figure 1.

	G			T			KE		
Region	r	MAD	RMSD	r	MAD	RMSD	r	MAD	RMSD
Pressure level of 1000 mb									
D	0.98	6	24	0.98	0.1	3.4	0.95	10	39
1	0.95	-3	9	0.78	2.5	3.0	0.51	13	17
2	0.97	9	13	0.92	-0.2	1.7	0.9	8	23
3	0.97	-15	25	0.96	2.5	4.2	0.83	12	27
4	0.95	-2	17	0.72	1.7	3.0	0.69	14	20
5	0.97	-6	14	0.64	2.4	3.5	0.79	20	22
Pressure level of 500 mb									
D	0.97	-1	23	0.99	-0.8	1.7	0.98	8	11
1	0.97	-2	6	0.81	-1.0	1.4	0.81	13	42
2	0.94	-1	8	0.81	-0.9	1.5	0.61	12	40
3	0.89	3	26	0.97	-1.0	1.8	0.93	7	111
4	0.74	2	16	0.88	-1.1	1.6	0.86	9	55
5	0.77	-1	10	0.79	-1.6	1.8	0.84	11	36